Bulletin of the Seismological Society of America, Vol. 104, No. 2, pp. –, April 2014, doi: 10.1785/0120130078

# The Profound Reach of the 11 April 2012 **M** 8.6 Indian Ocean Earthquake: Short-Term Global Triggering Followed by a Longer-Term Global Shadow

by Fred F. Pollitz, Roland Bürgmann, Ross S. Stein, and Volkan Sevilgen

Abstract The 11 April 2012 **M** 8.6 Indian Ocean earthquake was an unusually large intraoceanic strike-slip event. For several days, the global **M** ≥4.5 and **M** ≥6.5 seismicity rate at remote distances (i.e., thousands of kilometers from the mainshock) was elevated. The strike-slip mainshock appears through its Love waves to have triggered a global burst of strike-slip aftershocks over several days. But the **M** ≥6.5 rate subsequently dropped to zero for the succeeding 95 days, although the **M** ≤6.0 global rate was close to background during this period. Such an extended period without an **M** ≥6.5 event has happened rarely over the past century, and never after a large mainshock. Quiescent periods following previous large (**M** ≥8) mainshocks over the past century are either much shorter or begin so long after a given mainshock that no physical interpretation is warranted. The 2012 mainshock is unique in terms of both the short-lived global increase and subsequent long quiescent period. We believe that the two components are linked and interpret this pattern as the product of dynamic stressing of a global system of faults. Transient dynamic stresses can encourage short-term triggering, but, paradoxically, it can also inhibit rupture temporarily until background tectonic loading restores the system to its premainshock stress levels.

## Introduction

The 11 April 2012 **M** 8.6 earthquake was an exceptionally large strike-slip event that occurred within the oceanic lithosphere (McGuire and Beroza, 2012). It was followed by an increase in global seismicity rates at magnitudes 4.5 ≤ **M** ≤ 7.0 for several days (Pollitz *et al.*, 2012). A marked change in global seismicity rates occurred over six day periods pre- and postmainshock, as well as with respect to the measures of background rates (Pollitz *et al.*, 2012). We depict it at **M** ≥6.5 in Figure 1d, which indicates a briefly elevated rate (0.4 events/day for 10 days) relative to three 100 day periods before the event (averaging ∼0.1 events/day).

Although other great earthquakes have triggered smaller earthquakes and tremors worldwide, usually upon passage of the seismic waves (e.g., Prejean *et al.*, 2004; Velasco *et al.*, 2008; Gonzales-Huizar *et al.*, 2012), the global seismicity response to the Indian Ocean event is unique. It extends to large magnitudes (up to 7.0), and involves predominantly delayed triggered seismicity. This may be related to the high stress drop and large Love-wave excitation associated with the event (McGuire and Beroza, 2012; Meng *et al.*, 2012; Yue *et al.*, 2012), but much remains to be explained, especially the mechanism of delayed triggering.

The April 2012 earthquake was remarkable in another aspect. The brief acceleration in global seismic activity was followed by a nearly 100 day long quiescence at **M** ≥6.5 (Fig. 1e). We shall document that such a long period without a large earthquake is rare. This raises the question as to its association with the April 2012 mainshock, specifically whether the globally propagating seismic waves from the mainshock were capable of producing not only a brief acceleration, but also a longer-term quiescence.

A clue to the triggering power of the April 2012 event lies in the apparent triggering of a foreshock sequence ∼20 s prior to an **M** 3.9 dynamically triggered aftershock in Alaska (Tape *et al.*, 2013). This suggests that source patches that are close to failure may exhibit a gradual precursory slip prior to generating a larger triggered event. This lends support to a model of delayed dynamic triggering in which slow slip or small earthquakes cascade into a larger triggered event (Peng and Gomberg, 2010; Shelly *et al.*, 2011). We consider a variation of this model in which source areas close to failure are brought even closer to failure by propagating seismic waves, pushing a substantial fraction of them over a stress threshold. In order to explain the subsequent ∼100 day shutdown in **M** ≥6.5 activity, the model further postulates a dynamic shadow effect which can suppress seismicity even when many source areas are close to failure and are expected to rupture.

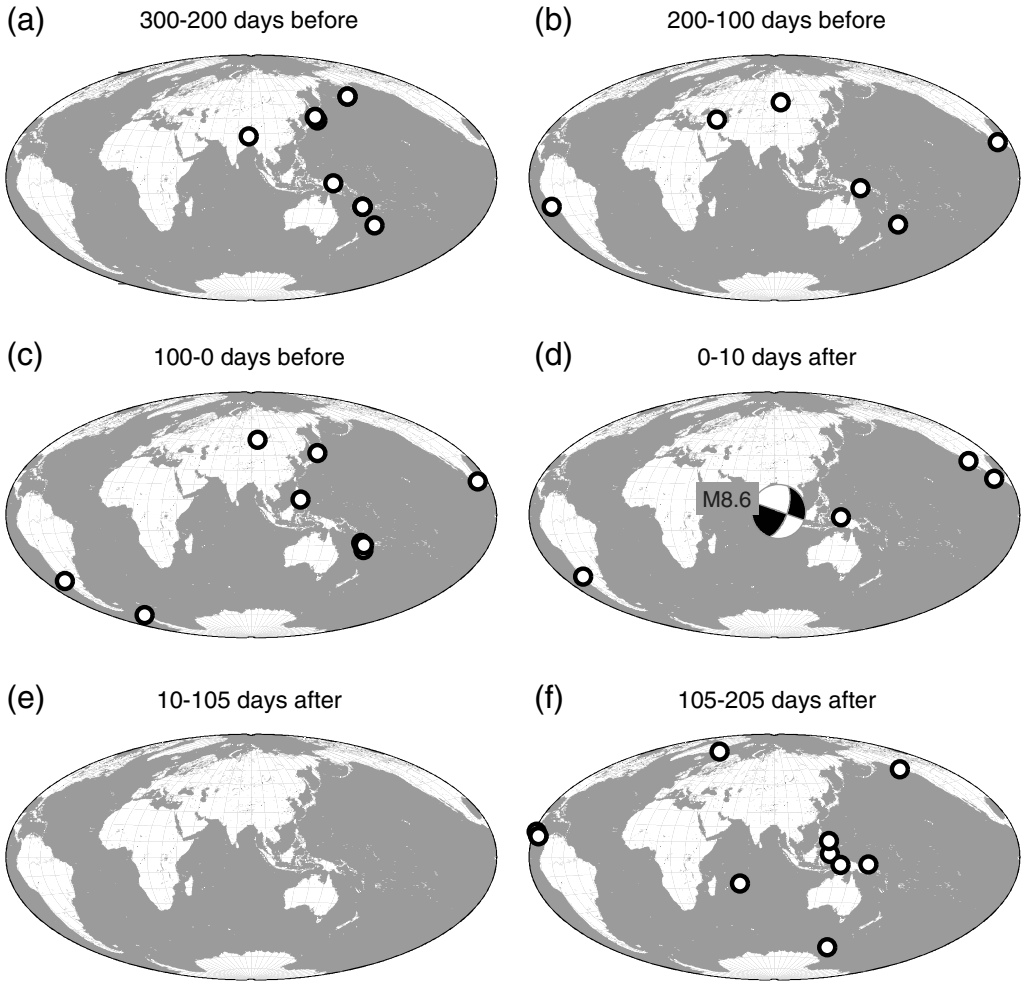


**Figure 1.** Remote global **M** ≥6.5 seismicity (0–100 km depth here and in subsequent figures) over the indicated time periods. Time is relative to the origin time of the 11 April 2012 Indian Ocean event. Remote events are defined as those > 1500 km from the epicenter of the 11 April 2012 Indian Ocean event (indicated in d).

In this study, we document both the postmainshock short-term (10 day) seismicity increase and the longer-term (subsequent 95 day) quiescence following the April 2012 Indian Ocean event. We shall establish that the 2012 mainshock is unique among large mainshocks over the past century in terms of the dearth of global seismicity during a long period following it. This motivates a discussion of its physical implications. Although any model based on a unique observation is speculative, a simple model of the global system of faults will be proposed. It will act both as a reference for rationalizing the post-2012 mainshock seismicity pattern as well as highlighting what makes this particular large mainshock different from many others which have preceded it.

## Postmainshock Acceleration

We use the National Earthquake Information Center (NEIC) catalog to document global seismicity patterns before and after the 11 April 2012 mainshock. We use reported moment magnitude $M_w$. Pollitz *et al.* (2012; their fig. S3) note that from 2002 to 2012 this catalog has a magnitude of completeness $M_c \sim 4.8$. A similar analysis using catalog events since 2009 suggests $M_c \sim 4.5$. This is consistent with the $M_c$ estimated for smaller regions based on comparisons of the NEIC catalog with local catalogs (e.g., Goslin *et al.*, 2012; Sevilgen *et al.*, 2012).

Figure 2 shows cumulative global **M** ≥4.5 earthquake counts for a 4.2 year long period in an unedited catalog. Increases in cumulative **M** ≥4.5 are well correlated with the occurrence of **M** ≥6.5 events (vertical dashed lines and open circles in Fig. 2, extended to **M** ≥6.4). Increases are particularly evident at the time of the 28 February 2010 **M** 8.8 Maule earthquake, 11 March 2011 **M** 9.0 Tohoku earthquake, and 11 April 2012 **M** 8.6 Indian Ocean earthquake. We also evaluate the same seismicity using a declustered catalog designed to remove local aftershocks from the largest mainshocks. The global catalog is edited such that all **M** <8.0 events occurring within one year following an **M** ≥8.0 event and within 1500 km of it are excluded. We refer to this as large-mainshock declustering. The resulting cumulative

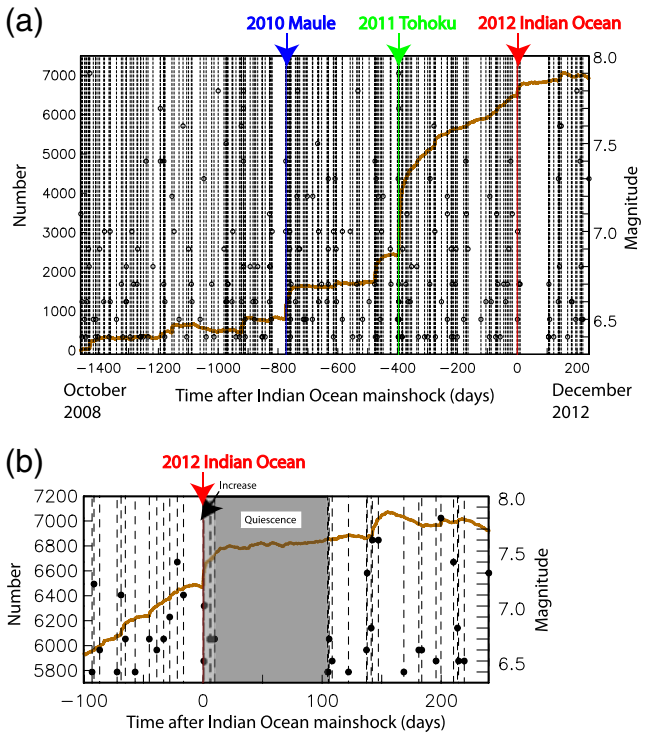


**Figure 2.** (a) Cumulative number of **M** ≥4.5 earthquakes reduced by 13 events/day. Time is relative to the origin time of the 11 April 2012 Indian Ocean event. The vertical dashed lines indicate times of **M** ≥6.4 events, with magnitudes given by corresponding open circles. Catalog is unedited (i.e., no 1500 km exclusion zones). Panel (b) is a close-up of (a) over the period from 100 days before to 240 days after the mainshock. The color version of this figure is available only in the electronic edition.

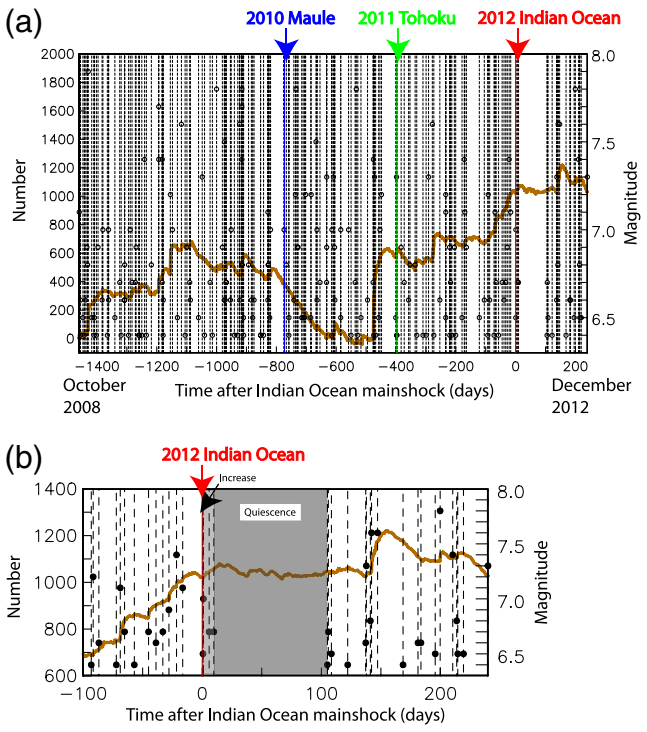


**Figure 3.** (a) Cumulative number of **M** ≥4.5 earthquakes reduced by 13 events/day. Time is relative to the origin time of the 11 April 2012 Indian Ocean event. The vertical dashed lines indicate times of **M** ≥6.4 events, with magnitudes given by corresponding open circles. Events are edited with large-mainshock declustering. Panel (b) is a close-up of (a) over the period from 100 days before to 240 days after the mainshock. A large mainshock occurring 475 days before the 11 April 2012 **M** 8.6 event is the 21 December 2010 **M** 7.4 event off Japan. It was followed by vigorous local aftershock activity that is retained because the **M** 7.4 event is not eliminated by the employed declustering. The color version of this figure is available only in the electronic edition.

global **M** ≥4.5 earthquake counts and occurrence times of **M** ≥6.5 events are shown in Figure 3. The declustering has removed local aftershocks from the Maule, Tohoku, and Indian Ocean events (and all other **M** ≥8.0 mainshocks). An increase at **M** ≥6.5 following the Indian Ocean event, however, is seen regardless of how the catalog is edited (e.g., part b of these figures) because these larger events are remote.

A diagnostic property of the globally triggered seismicity identified by Pollitz *et al.* (2012) was the predominance of strike-slip events, presumably because the strongest seismic energy radiated globally was transmitted by the Love waves, which have a high potential for dynamically triggering strike-slip events (Hill, 2010). Figure 4a,b shows the fraction $\gamma(t)$ of **M** ≥5.0 remote events with strike-slip focal mechanisms relative to the total number of **M** ≥5.0 remote events cumulatively up to time $t$, derived from the Global CMT catalog (the Global Centroid Moment Tensor Project [see Data and Resources]; Dziewonski *et al.*, 1981; Ekström *et al.*, 2012). The times of strike-slip events and all events used to construct $\gamma(t)$ are shown in Figure 4c and 4d, respectively. In the days following the 11 April 2012 mainshock, the values of $\gamma$ are systematically higher than the background value of 0.24 determined from several years of pre-April 2012 seismicity. Figure 4 includes the pattern $\gamma(t)$ derived from cumulative strike-slip events counting backward in time from the 11 April 2012 mainshock. In contrast with the postmainshock pattern, the premainshock pattern fluctuates about the background and is not systematically distinct from it for a prolonged period.

The **M** ≥5.5 remote global seismicity was elevated at 99% significance for the first two days following the event based on rate changes and absolute rates derived from the first two days postearthquake period (Pollitz *et al.*, 2012). The anomalous seismicity rates persist out to 10 days following the mainshock at **M** ≥5.5. This is based on comparing the observed seismicity rate increase over the first 10 days with empirical probability distributions derived from all 10 day periods following **M** ≥7 mainshocks over the 20 years preceding the April 2012 event. Figure 5 reveals that the observed seismicity rate exceeds the 95% tail of the empirical probability distributions at magnitude thresholds of 5.5 and greater.

## Transition from Triggered to Background Seismicity

The initial post-2012 mainshock acceleration was short lived, and we aim to quantify the transition to background

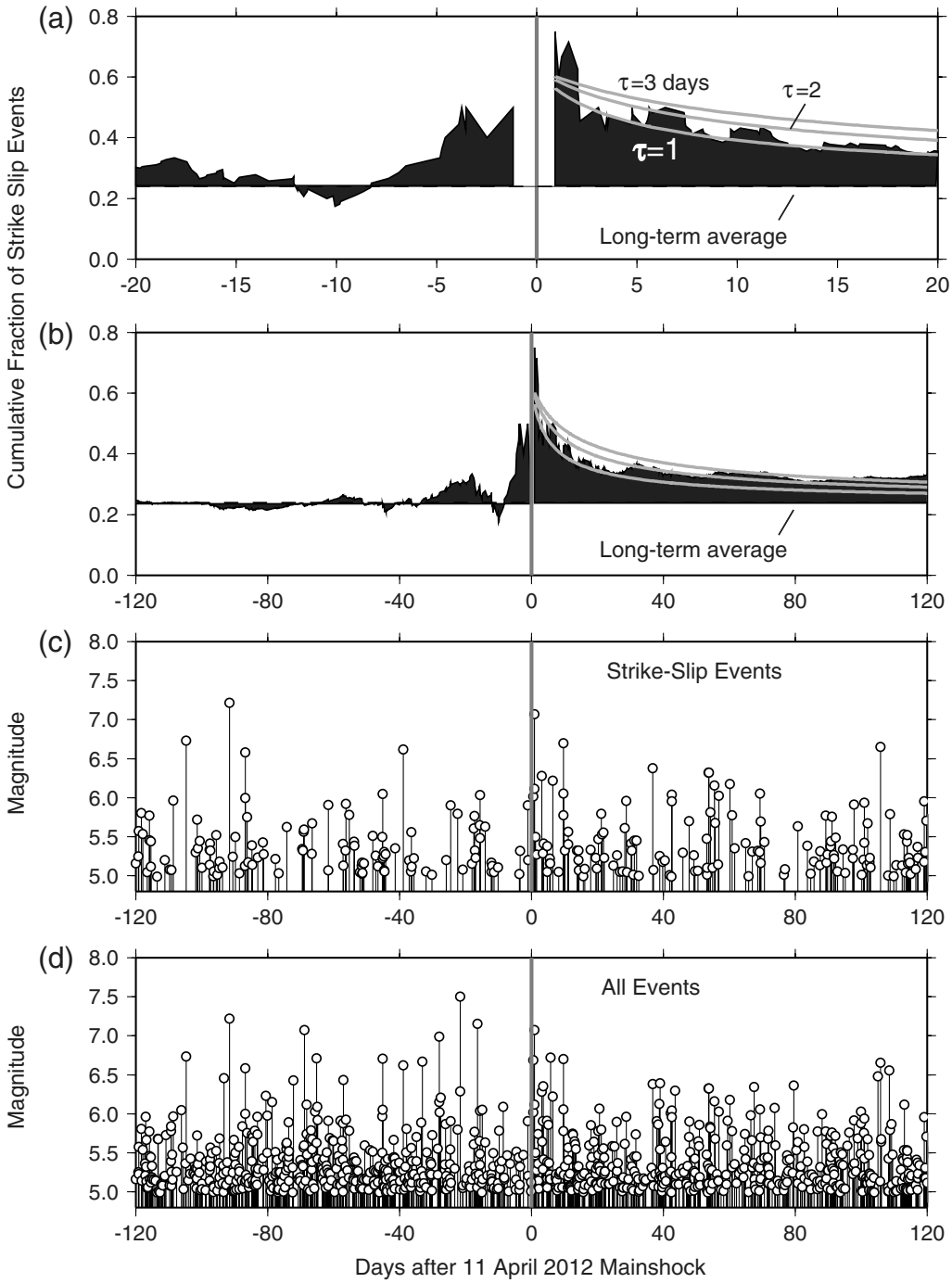


**Figure 4.** (a, b) Cumulative fraction of $\mathbf{M} \geq 5.0$ strike-slip events (defined as those with the plunge of the neutral axis $> 60°$) relative to the total number of global events averaged over time, calculated in separate periods pre- and post-2012 mainshock. Panel (a) is a close-up of (b) over 20 day time periods. Superimposed in gray are model curves for Omori decay of the strike-slip global events, using values $A = 10$ and $\tau = 1$, 2, or 3 days in equation (4). The premainshock cumulative curve is derived counting time backward from the 11 April 2012 mainshock (indicated with thick vertical gray line). Lower panels show occurrence times and magnitudes of (c) $\mathbf{M} \geq 5.0$ strike-slip events, and (d) all events during this time period. All events are constrained to be $> 1500$ km away from the 11 April 2012 epicenter. All data in this figure are from the Global CMT catalog.

seismicity. Time-dependent $\gamma$ in Figure 4 exhibits an Omori-like decay. We explain this with a model in which the rate of strike-slip global earthquakes is

$$r(t) = r_0\left[1 + A\left(1 + \frac{t}{\tau}\right)^{-1}\right], \qquad (1)$$

in which $r_0$ is the background rate of global strike-slip $\mathbf{M} \geq 5.0$ earthquakes, and $A$ and $\tau$ are constants. The cumulative number of strike-slip events up to time $t$ after the mainshock is

$$N_{ss}(t) = \int_0^t r(t')dt' = r_0 t\left[1 + \frac{A\tau}{t}\ln\left(1 + \frac{t}{\tau}\right)\right]. \qquad (2)$$

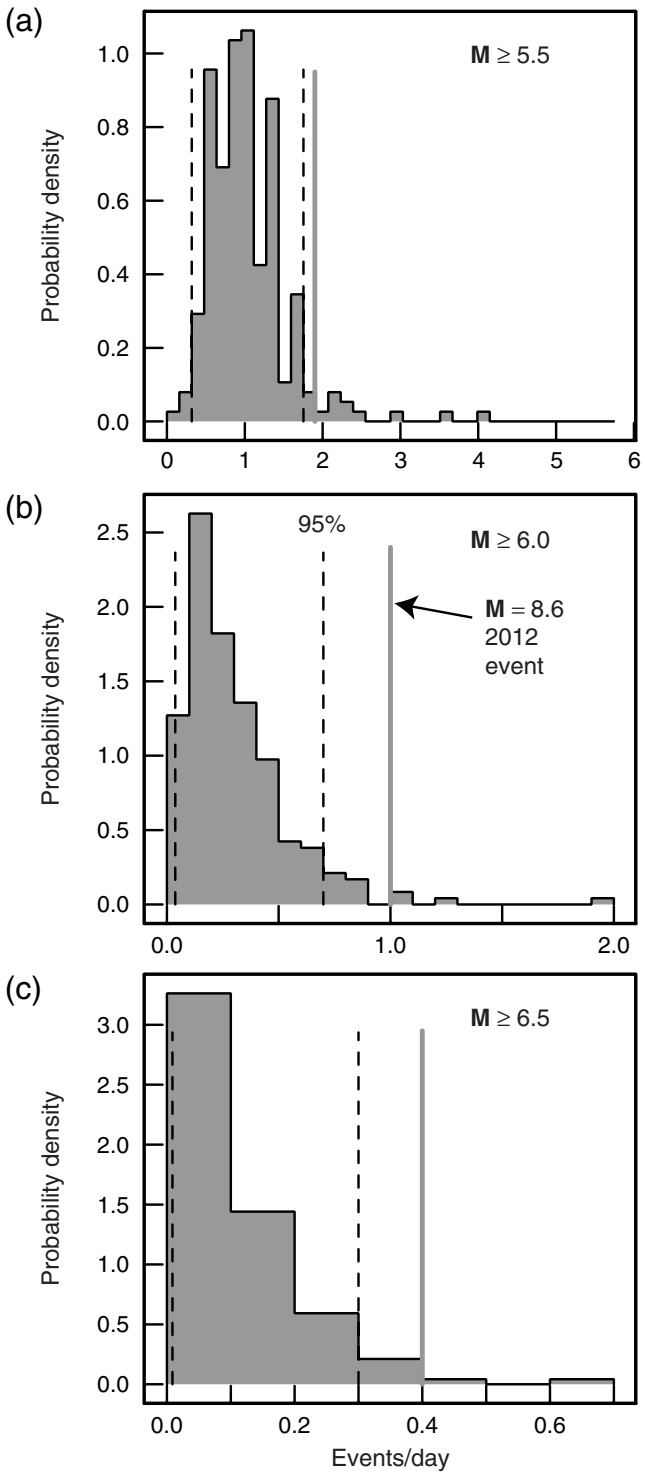


**Figure 5.** Empirical probability density functions of the remote seismicity rate above a given magnitude during the 10 days following an **M** ≥7 mainshock. They are calculated using the sampling procedure described in the Methods section of Pollitz *et al.* (2012); 243 **M** ≥7 mainshocks during the 20 years preceding the April 2012 Indian Ocean event are employed. All seismicity rates are remote in the sense that events occurring after a given **M** ≥7 mainshock are constrained to lie outside a spherical cap of radius 1500 km centered on that mainshock. The dashed lines indicate the 5% and 95% tails of the distributions, and the vertical gray line denotes the observed remote seismicity rate during the 10 days following the April 2012 event.

Let $N_{\text{total}}(t)$ be the total cumulative number of **M** ≥5.0 remote earthquakes between time 0 and $t$ after the mainshock. If we make the crude assumption that most of the postmainshock acceleration is due to preferential triggering of strike-slip events, then

$$N_{\text{total}}(t) \approx N_{ss}(t) + \left(\frac{1}{0.24} - 1\right) r_0 t. \tag{3}$$

This yields an expression for $\gamma$:

$$\gamma(t) = \frac{N_{ss}(t)}{N_{\text{total}}(t)} = \left[1 + \frac{3.17}{1 + \frac{A\tau}{t}\ln(1 + \frac{t}{\tau})}\right]^{-1}. \tag{4}$$

Gray curves in Figure 4a,b show the predictions of equation (4) for $A = 10$ and $\tau = 1$, 2, or 3 days. The fit to the observed $\gamma$ indicates that increased global strike-slip activity decayed with an Omori time constant $\tau \approx 1$–2 days, consistent with a gradual transition from triggered to background events within days following the 2012 mainshock. However, although this informs us on how long triggered remote events persisted, it does not completely describe the transition of earthquake rates, which is magnitude dependent in ways described in the next two sections.

## Postmainshock Quiescence

This initial acceleration in global earthquake rates following the 11 April 2012 mainshock (Fig. 1d), including seismicity at large magnitude up to **M** 7.0, is unusual. Even more unusual is the quiescence in **M** ≥6.5 seismicity during the following 95 days—from 21 April to 26 July 2012 (Fig. 1e). This pattern is remarkable when compared with the three 100 day long periods premainshock and the subsequent 100 day long period postmainshock (Fig. 1a,b,c,f). The pattern is recast with the 2008–2012 history of **M** ≥6.5 events in Figures 2 and 3, which use no catalog editing or large-mainshock declustering, respectively. The observed 95 day period is robust with respect to possible local aftershocks: it remains even when global seismicity rates are evaluated without any catalog editing.

A similar perspective on the shutdown in global seismicity is revealed in Figure 6, which shows the cumulative number of **M** ≥6.5 events using the NEIC catalog with large-mainshock declustering. The solid gray line with slope 0.089 events/day represents the 30 year background rate. When this rate is extrapolated to 105 days postmainshock, 9.4 **M** ≥6.5 events should have occurred during this time; only four occurred (i.e., those of the first 10 days), leaving an apparent gap of 5.4 events. This implies at face value a gap equivalent to 60 days' worth of global **M** ≥6.5 seismic activity.

To address how often an extended globally quiet period has occurred, we make use of the International Seismological Centre-Global Earthquake Model (ISC-GEM) catalog, which begins in 1900 and is intended to supplant the Centennial catalog (Engdahl and Villaseñor, 2002). The ISC-GEM Global

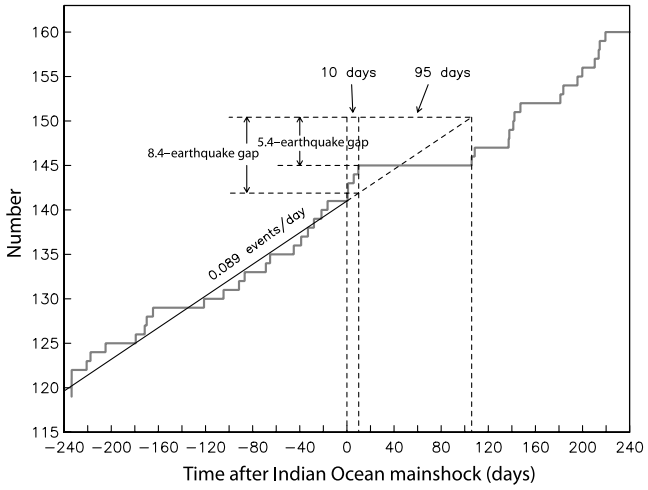


**Figure 6.** Cumulative number of **M** ≥6.5 events from 240 days before to 240 days after the April 2012 Indian Ocean mainshock using the NEIC catalog with large-mainshock declustering. (The pattern without declustering is nearly identical, with the addition of only three events.) Although a 5.4 event gap apparently results when examining the budget of **M** ≥6.5 events expected to occur within 105 days after the mainshock, the four events, which occurred within the first 10 days—because they are dynamically triggered—contribute little to the budget of expected **M** ≥6.5 earthquake productivity for this time period. This results in an effective 8.4 earthquake gap during the 95 day quiescent period. The background rate of 0.089 events/day is based on the 30 year catalog NEIC catalog and ISC-GEM catalog.

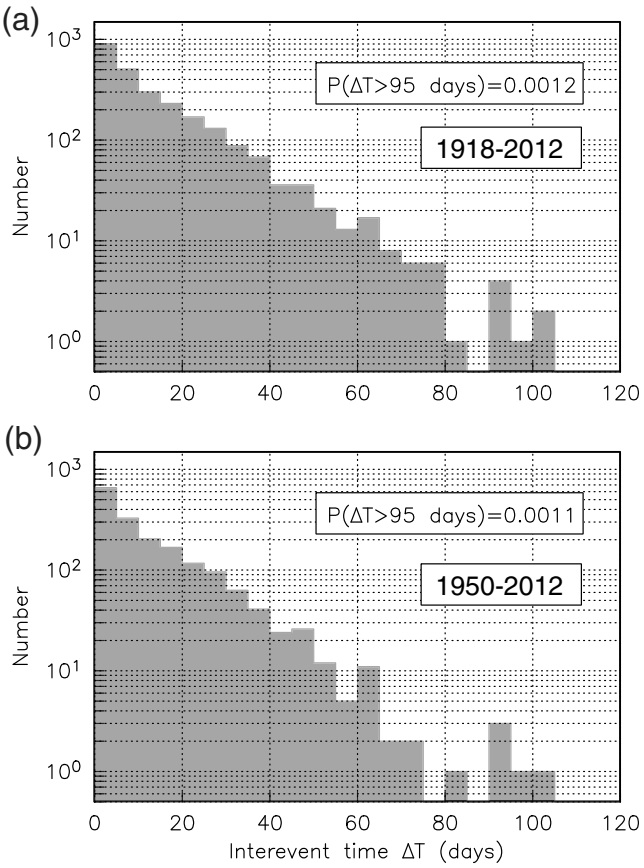


**Figure 7.** Histograms of global **M** ≥6.5 interevent times $\Delta T$ using the ISC-GEM catalog for the periods (a) 1918 to 11 April 2012 and (b) 1950 to 11 April 2012. Large-mainshock declustering is applied. Probability of $\Delta T$ exceeding 95 days is indicated in each case.

Instrumental Earthquake Catalogue (Storchak *et al.*, 2012) relocated 19,000 earthquakes during 1900–2009; it is the result of a special effort to adapt and substantially extend and improve currently existing bulletin data. A million phase records were digitized, and all earthquakes were relocated using Bondár and Storchak (2011). Approximate completeness is **M** ≥7.50 since 1900, **M** ≥6.25 since 1918, and **M** ≥5.50 since 1965.

Analysis of both the 30 year (1982–2012) NEIC catalog and the ISC-GEM catalog shows the background rate of remote **M** ≥6.5 earthquakes is 0.105 events/day without editing and 0.089 events/day with large-mainshock declustering. Using the latter value and assuming a Poissonian distribution for event occurrence, this implies that the probability of realizing a 95 day interval with no **M** ≥6.5 events is $\approx \exp[-8.45] = 2 \times 10^{-4}$. The rarity of this is confirmed by compilation of **M** ≥6.5 remote interevent times $\Delta T$ using the ISC-GEM catalog. To more accurately represent the occurrence of remote **M** ≥6.5 and reduce any possible bias toward low $\Delta T$ in the historical catalog, we use large-mainshock declustering. Figure 7 shows there are only three instances in which interevent periods were longer than 95 days during the past century. The probability of realizing $\Delta T$ longer than 95 days is 0.0012 for the past 95 years (Fig. 7a) and 0.0011 for the past 59 years (Fig. 7b).

The empirical probabilities for $\Delta T > 95$ days discussed above are based on retrospective analysis using the observed interval of quiescence. Retrospective analysis can make an identified phenomenon appear significant when in reality the phenomenon is bound to occur given a long enough observation trial (e.g., Shearer and Stark, 2011). In the present case, the fact that $\Delta T$ as long as 100 days has been observed a few times during the past century indeed makes a single observation of such an interval not necessarily significant. What is remarkable about the observation is that it follows a very large seismic event by only several days. To put this in perspective, we examine the pattern of **M** ≥6.5 interevent times $\Delta T$ in terms of the elapsed time since the last large mainshock (i.e., that mainshock preceding the first of two consecutive **M** ≥6.5 events), which we restrict to mainshocks of **M** ≥8.0. Each such pair of **M** ≥6.5 events can be represented on a plot with $\Delta T$ on one axis and the elapsed time since the last large mainshock on the other axis, as shown schematically in Figure 8a,b. This pattern is determined with large-mainshock declustering, which tends to encourage longer $\Delta T$ in the historical catalog and thereby make the post-Indian Ocean quiescent period less anomalous. This pattern, shown in Figure 8c, reveals that $\Delta T$ bears no systematic relationship with elapsed time since a large event. This elapsed time since the last large mainshock

approximately follows a uniform distribution, and no physical connection between the elapsed time and a long interevent time is warranted. Among the very large ($\mathbf{M} \geq 8.5$) events, the April 2012 mainshock stands apart because of its unusually long $\Delta T$ and short (10 day) elapsed time since the mainshock. The unusually long interevent times for the April 2012 mainshock versus others over the past century are also manifested at a magnitude threshold of 6.25 (Fig. 8d), although it is weaker than at the larger magnitude threshold, and other past large mainshocks are also associated with unusually long $\Delta T$ fairly soon after they occurred (e.g., the 1964 **M** 9.3 Alaska and 1952 **M** 8.9 Kamchatka earthquakes). We find that this pattern is absent at a magnitude threshold of 6.0, showing that the observed phenomenon is confined to global events of magnitude $\gtrsim 6.25$.

A similarly large $\Delta T$ and short elapsed time are associated with the **M** 8.1 Tonankai earthquake of 7 December 1944 in the southern Nankai trough, which plots close to the 2012 event in Figure 8c. There is a $\Delta T = 103$ day gap between two subsequent $\mathbf{M} \geq 6.5$ events—the 12 December 1944 **M** 6.51 event along the Aleutian arc and 23 March 1945 **M** 6.83 event along the Pacific–Antarctic Ridge. Although there are four $\mathbf{M} \geq 6.5$ events globally during the intervening time, all of them are within 1500 km of the 7 December 1944 mainshock and therefore removed with the remoteness criterion. However, the Centennial Catalog (Engdahl and Villaseñor, 2002) contains an additional six events at remote distance from the 7 December 1944 mainshock during the intervening time with body-wave magnitude $m_b$ ranging from 6.6 to 7.2. In the ISC-GEM catalog these events are assigned either an $M_w$ less than 6.5 or are assigned no magnitude. These additional events merit further examination because $m_b$ tends to underestimate $M_w$, especially at larger magnitude (Kanamori, 1983). Thus the apparently large $\Delta T$ for the 7 December 1944 event may be an artifact of uncertain $M_w$ assignments associated with a lapse in seismic event detection during World War II.

To put the employed large-mainshock declustering into perspective, we note it is applied for the sole purpose of making the 2012 mainshock appear less remarkable when compared with other events. Relative to modeling of an unedited catalog, the declustering procedure at **M** 8.0 pushes interevent times in Figure 7 to the right (i.e., higher). Similarly it pushes the interevent times associated with all past large mainshocks in Figure 8 to the right. A lower threshold (e.g., **M** 7.5) would make the 2012 mainshock stand out even more starkly. That is because the declustering has no effect on the interevent times documented for the post-2012 mainshock period. That point is also made with Figures 2 and 3: the long quiescent period remains even if the catalog is unedited. Similarly, the quiescent period remains if the radius is decreased to 1000 km, and decreasing this radius would also push interevent times in Figures 7 and 8 to the left, and thus make the 2012 quiescent period appear even more remarkable.

## Magnitude–Frequency Statistics

We wish to compare the April 2012 short-term increase and longer-term decrease with background rates of remote seismicity. Employing the NEIC catalog and following Pollitz *et al.* (2012), this background is derived from all 10 day intervals following $\mathbf{M} \geq 7$ events during the four years preceding the April 2012 Indian Ocean mainshock; the epicenter of each $\mathbf{M} \geq 7$ event is the center of an exclusion zone of radius 1500 km applied to each subsequent 10 day long period. Large-mainshock declustering could be superimposed as an additional filter, but our prescription for the background rates already removes the majority of local aftershocks (and it is consistent with the measures defined below that we shall compare it with). This background is shown with the filled circle symbols in Figure 9f.

Remote events during the 10 days following the April 2012 event are similarly constrained to be $> 1500$ km from the 2012 Indian Ocean epicenter. They are shown with the open triangle symbols in Figure 9f. Compared with background seismicity rates, the short-term (0–10 days postmainshock) activity is elevated.

We evaluate the global earthquake activity during the 10–105 days post-Indian Ocean mainshock period and excluding those events $< 1500$ km from the April 2012 epicenter. At $\mathbf{M} \geq 4.5$, the earthquake rates during the 10–105 days post-Indian Ocean mainshock period is similar to the background in terms of its magnitude–frequency statistics (Fig. 9f). The 10–105 days postmainshock period departs from background at $\mathbf{M} > 6.0$ and lacks any $\mathbf{M} \geq 6.4$ events.

Magnitude–frequency statistics are similarly derived for other very large ($\mathbf{M} \geq 8.5$) mainshocks of the past 10 years: 2004 **M** 9.2 Sumatra–Andaman, 2005 **M** 8.7 Nias, 2007 **M** 8.5 Sumatra, 2010 **M** 8.8 Maule, Chile, and 2011 **M** 9.0 Tohoku. Background rates over the four years preceding the mainshock, and 0–10 day and 10–105 day postmainshock intervals are used as for the 2012 mainshock, and earthquakes within 1500 km of each respective mainshock epicenter are excluded. The results presented for these other mainshocks in Figure 9a–e show neither a significant short-term rate increase nor a longer-term decrease; the longer-term seismicity rates (open circle symbols in the plots) generally do not saturate at any magnitude, that is, no quiescence at a longer period. A possible post-2004 Sumatra quiescence at $\mathbf{M} \geq 6.9$ is revealed by Figure 9a. How this compares with the post-2012 quiescence at $\mathbf{M} \geq 6.5$ may be ascertained by generating histograms of $\mathbf{M} \geq 6.9$ remote interevent times $\Delta T$ using the ISC-GEM catalog as was done in Figure 7 at $\mathbf{M} \geq 6.5$. We find that the probability of an interevent time $\Delta T > 95$ days is 0.035 and 0.032 for the 1918–2012 and 1950–2012 periods, respectively. This probability is ~30 times greater than that for $\Delta T > 95$ days at $\mathbf{M} \geq 6.5$, so the post-2004 quiescence is far less significant than the post-2012 quiescence. Although the 10–105 day postmainshock period is used to test for a possible decrease in all cases, this pattern is robust with respect to other choices (e.g. a period

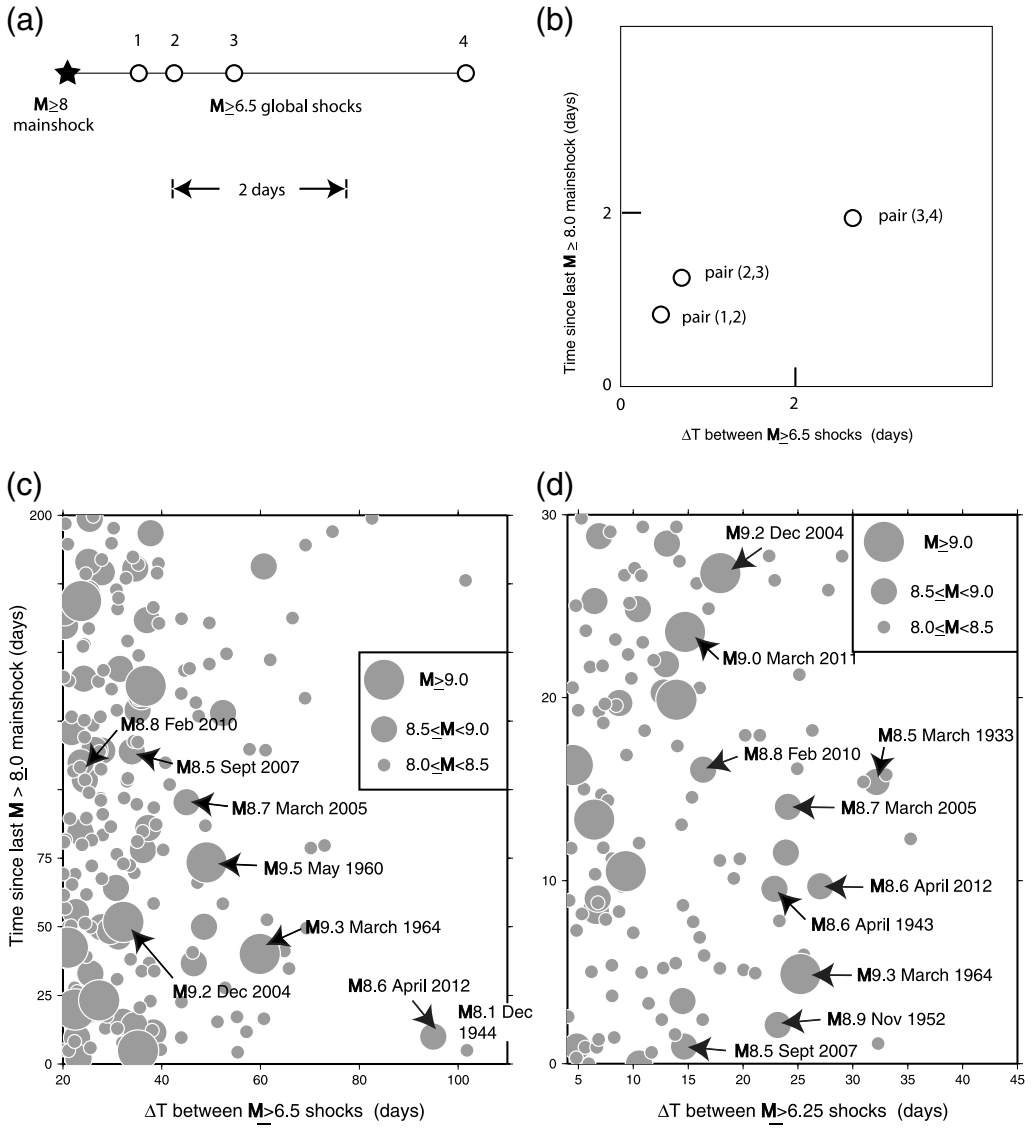


**Figure 8.** (a) Four consecutive hypothetical **M** ≥6.5 shocks and the last **M** ≥8.0 shock preceding them are shown in a schematic timeline. (b) The resulting three pairs of consecutive **M** ≥6.5 shocks are represented by their interevent time $\Delta T$ (abscissa) and the time from the **M** ≥8.0 shock to the first **M** ≥6.5 shock in the given pair (ordinate). (c) **M** ≥6.5 and (d) **M** ≥6.25 interevent time $\Delta T$ versus the time since the last **M** ≥8.0 mainshock preceding the first of two consecutive **M** ≥6.5 (or 6.25) events. Events are extracted from the 1918–July 2012 ISC-GEM catalog. Large-mainshock declustering is applied. Data for notable past large mainshocks are indicated; only that pair of consecutive **M** ≥6.5 (or 6.25) events associated with the largest $\Delta T$ for that particular mainshock is indicated. In (c), no data are present for the March 2011 Tohoku event because $\Delta T$ for post-Tohoku seismicity does not exceed 20 days prior to the occurrence of the next global **M** ≥8.0 mainshock. Global seismic station reporting was exceptionally poor during World War II, and so $\Delta T$ for the 1944 **M** 8.1 shock is probably lower than shown.

extending anywhere from 50 to 200 days postmainshock). This confirms the pattern suggested by the interevent statistics (Fig. 8) that the 2012 mainshock is unique among the recent well-documented very large mainshocks.

## Implications for Earthquake Physics

In the Appendix we develop a statistical model of global seismicity motivated by the post-2012 mainshock observations. This model involves tens of thousands of source patches capable of **M** ≥6.5 ruptures, steady loading of each fault in the system, and the supposition of a random distribution of stress states between complete stress drop and near failure with a critical strain threshold of $\epsilon_{\rm crit}$. It is designed to explain both the 10 day increase and subsequent 95 day decrease in global **M** ≥6.5 seismicity rates. Two consequences of the model are:

1. roughly 6% of those patches that would have been temporarily strained above $\epsilon_{\rm crit}$ by the seismic waves did actually rupture;
2. of those that did not rupture, roughly 88% were somehow removed from the eligible pool of potentially failing sites

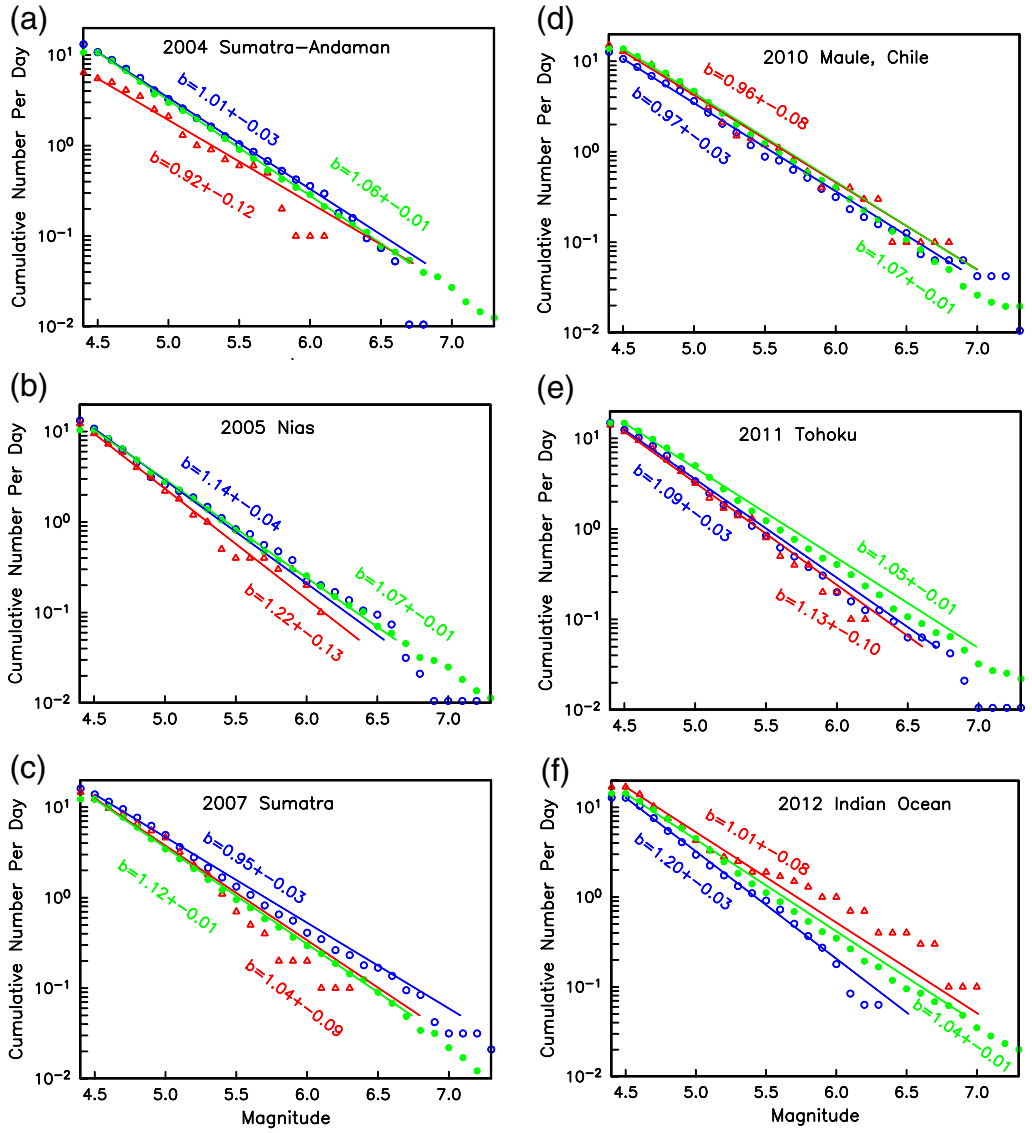


**Figure 9.** Cumulative number of remote events as a function of magnitude, normalized to the time interval being considered, using the NEIC catalog. The filled circle symbols represents background remote events calculated using four years of seismicity prior to the given mainshock. The triangle symbols represent remote events during the period 0 to 10 days following a given mainshock. The diamond symbols represent remote events during the period 10–105 days following the given mainshock. The lines indicate the corresponding fit to a linear magnitude–frequency relationship with *b*-values calculated using maximum likelihood estimation. (a) 26 December 2004 **M** 9.2 Sumatra–Andaman, (b) 28 March 2005 **M** 8.7 Nias, (c) 12 September 2007 **M** 8.5 Sumatra, (d) 27 February 2010 **M** 8.8 Maule, Chile, (e) 11 March 2011 **M** 9.0 Tohoku, and (f) 11 April 2012 **M** 8.6 Indian Ocean earthquake. Epicenters within 1500 km of each respective mainshock are excluded. The color version of this figure is available only in the electronic edition.

on a 100 day timescale, regardless of the fact that they had been previously close to failure.

This removal of apparently close-to-failure sites from being capable of rupturing at the **M** ≥6.5 level is surprising, and might have two possible explanations:

1. transient mainshock stresses may have changed the state of close-to-failure patches, delaying an ongoing process of cascade to failure;
2. dynamic changes in permeability could reduce the effective stress along a fault, for example by changing the distribution of pore fluid pressures and hence effective coefficient of friction along the patch.

The first explanation, involving changing the state of a fault by dynamic stresses, for example, through an increase in the mean critical slip distance $D_c$, has been previously proposed by Parsons (2005) as a mechanism for delayed triggering. We suggest that it is a possible mechanism for delaying a rupture even if it was impending in the absence of transient dynamic stresses. In the context of rate-and-state friction theory, Parsons (2005) notes that although seismically

induced reductions in $D_c$ may occur (and lead to increased seismicity rates), it is also physically plausible that dynamic stresses could increase $D_c$ (and lead to reduced seismicity rates).

The second explanation is based on the fact that faults tend to have a low-permeability core surrounded by a high-permeability damage zone (Caine *et al.*, 1996). Transient stresses may suddenly reduce permeability on a fault, temporarily allowing local pore pressure changes, which may trigger earthquakes (e.g., Brodsky *et al.*, 2003). The recovery process after an initial perturbation, however, will act to reduce fault zone permeability (section 4 of Manga *et al.*, 2012). Although the recovery process is thought to return the fault zone to its pre-existing state, it is conceivable that a fault zone may undergo a net decrease in effective stress, possibly by expulsion of fluids from the fault zone during the initial perturbation.

Either of the two proposed processes, if truly applicable, would have been stimulated by dynamic stress from the 2012 mainshock, but not by any previous large mainshocks over the past century. And it would affect primarily source areas capable of $\mathbf{M} \gtrsim 6.25$ ruptures, but not smaller ruptures. The dynamic stresses associated with the 2012 mainshock were commensurate with that of any other historical event, and, where directly comparable with larger magnitude events such as the 2004 **M** 9.2 Sumatra earthquake, were larger (e.g., figure S-10 of Pollitz *et al.*, 2012). This is likely because of its compact rupture area and consequently short rupture duration and high stress drop relative to other ruptures of similar net seismic moment (McGuire and Beroza, 2012; Meng *et al.*, 2012; Yue *et al.*, 2012). Moreover, as a rare strike-slip event the 2012 mainshock excited primarily Love waves, rather than the Rayleigh waves that result from thrust events that predominate very large mainshocks. One might propose that Love waves are more effective than Rayleigh waves at stimulating the above processes, although this appears unlikely based on evidence from dynamic triggering of smaller events (Velasco *et al.*, 2008). At a given period, Love waves are of longer wavelength, and this may be related to the effect on seismicity pattern preferentially at $\mathbf{M} \gtrsim 6.25$.

## Conclusions

The 11 April 2011 **M** 8.6 earthquake is a unique seismic event in terms of the ensuing global seismic activity, characterized by a brief acceleration followed by a very long shutdown in $\mathbf{M} \geq 6.5$ seismicity. Its uniqueness is documented with comparison of post-2012 mainshock $\mathbf{M} \geq 6.5$ interevent times with interevent times following all large mainshocks over the past century, as well as comparison among magnitude–frequency statistics of postmainshock epochs following all $\mathbf{M} \geq 8.5$ mainshocks of the past decade. We believe that the early acceleration and subsequent quiescence are related and are the product of dynamic stressing from the mainshock. Using a 1D model of stressing of the global system of faults subject to a simple failure criterion, we find that (1) a small fraction of the reservoir of available close-to-failure patches was brought to failure, leading to the short-term seismicity rate increase; and (2) most other patches that might have been brought to failure during the subsequent 95 days were made temporarily incapable of sustaining a $\mathbf{M} \geq 6.5$ rupture. The first finding is a consequence of the transient stressing of close-to-failure patches temporarily above their failure threshold. The second finding is surprising and, if true, would imply that transient dynamic stressing from a large distant event can change the state of a fault such as to temporarily inhibit a large rupture.

This calls into question the notion that dynamic stresses can only increase earthquake rates rather than inhibit them. This has been used as the basis for discriminating between the mechanisms of dynamic stressing and the static stress change (e.g., Gomberg *et al.*, 1998; Felzer and Brodsky, 2005; Toda *et al.*, 2012). Our results for one **M** 8.6 mainshock suggest that dynamic stresses lead to increased global seismicity rates in the short term (everywhere that dynamic stresses are sufficiently high) and are thus consistent with this assumption. The idea that a dynamic stress shadow can develop over a longer time scale is suggested by our results, but needs to be confirmed by additional studies at regional scales. This could be done by repeating the analysis of Parsons and Velasco (2011) at intermediate distances from the largest ($\mathbf{M} \geq 8$) earthquakes in their dataset. It also could be accomplished by revisiting cases at which clear short-term increases are explicable with dynamic stressing (e.g., Kilb *et al.*, 2000; Gomberg *et al.*, 2003; Brodsky and Prejean, 2005; Hill and Prejean, 2007).

## Data and Resources

Seismic hypocenters and magnitudes were provided by the National Earthquake Information Center (NEIC) catalog, the International Seismological Centre-Global Earthquake Model (ISC-GEM) catalog, and the Global Centroid Moment Tensor (CMT) catalog. The Global CMT Project database was searched using www.globalcmt.org/CMTsearch.html (last accessed July 2013). The ISC-GEM catalog is a component of the Global Earthquake Model effort at http://www.globalquakemodel.org (last accessed April 2013).

## Acknowledgments

We thank Jeanne Hardebeck and Ruth Harris for their internal reviews of a preliminary draft. This paper has benefitted from the constructive criticisms of three anonymous reviewers and the Associate Editor Luis Angel Dalguer.

## References

Bird, P., Y. Kagan, and D. Jackson (2002). Plate tectonics and earthquake potential of spreading ridges and oceanic transform faults, in, *Plate Boundary Zones*, S. Stein and J. Freymueller (Editors), Vol. 30. American Geophysical Union, Washington, D.C., 203–218.

Bondár, I., and D. Storchak (2011). Improved location procedures at the international seismological centre, *Geophys. J. Int.* **186,** 1220–1244.

Brodsky, E. E., and S. G. Prejean (2005). New constraints on mechanisms of remotely triggered seismicity at Long Valley Caldera, *J. Geophys. Res.* **110,** no. B04302, doi: 10.1029/2004JB003211.

Brodsky, E. E., E. Roeloffs, D. Woodcock, I. Gall, and M. Manga (2003). A mechanism for sustained groundwater pressure changes induced by distant earthquakes, *J. Geophys. Res.* **108,** 2390, doi: 10.1029/2002JB002321.

Caine, J. S., J. P. Evans, and C. B. Forster (1996). Fault zone architecture and permeability structure, *Geology* **24,** 1025–1028.

Dziewonski, A. M., T.-A. Chou, and J. H. Woodhouse (1981). Determination of earthquake source parameters from waveform data for studies of global and regional seismicity, *J. Geophys. Res.* **86,** 2825–2852.

Ekström, G., M. Nettles, and A. M. Dziewonski (2012). The global CMT project 2004–2010: Centroid-moment tensors for 13,017 earthquakes, *Phys. Earth Planet. Int.* **200/201,** 1–9, doi: 10.1016/j.pepi.2012.04.002.

Engdahl, E. E., and A. Villaseñor (2002). Global seismicity: 1900–1999, in *International Handbook of Earthquake and Engineering Seismology*, W. H. K. Lee (Editor), Academic, Amsterdam, doi: 10.1016/S0074-6142(02)80244-3.

Felzer, K. R., and E. E. Brodsky (2005). Testing the stress shadow hypothesis, *J. Geophys. Res.* **110,** doi: 10.1029/2004JB003277.

Gomberg, J., M. L. Blanpied, and N. M. Beeler (1998). Earthquake triggering by transient and static deformation, *J. Geophys. Res.* **103,** 24,411–24,426.

Gomberg, J., P. Bodin, and P. A. Reasenberg (2003). Observing earthquakes triggered in the near field by dynamic deformations, *Bull. Seismol. Soc. Am.* **93,** 118–138.

Gonzales-Huizar, H., A. A. Velasco, Z. Peng, and R. R. Castro (2012). Remote triggered seismicity caused by the 2011 M 9.0 Tohoku-Oki, Japan earthquake, *Geophys. Res. Lett.* **39,** L10302, doi: 10.1029/2012GL051015.

Goslin, J., J. Perrot, J.-Y. Royer, and C. Martin (2012). Spatiotemporal distribution of the seismicity along the Mid-Atlantic Ridge north of the Azores from hydroacoustic data: Insights into seismogenic processes in a ridge-hot spot context, *Geochem. Geophys. Geosyst.* **13,** Q02010, doi: 10.1029/2011GC003828.

Hill, D. P. (2010). Surface-wave potential for triggering tectonic (nonvolcanic) tremor, *Bull. Seismol. Soc. Am.* **100,** 1859–1878.

Hill, D. P., and S. Prejean (2007). Dynamic triggering, in *Treatise on Geophysics*, G. Schubert (Editor), Vol. 4, Earthquake Seismology. Elsevier, Amsterdam, 258–288.

Kanamori, H. (1983). Magnitude scale and quantification of earthquakes, *Tectonophysics* **93,** 185–199.

Kilb, D., J. Gomberg, and P. Bodin (2000). Triggering of earthquake aftershocks by dynamic stresses, *Nature* **408,** 570–574.

Manga, M., I. Beresnev, E. E. Brodsky, J. E. Elkhury, D. Elsworth, S. E. Ingebritsen, D. C. Mays, and C.-Y. Wang (2012). Changes in permeability caused by transient stresses: Field observations, experiments, and mechanisms, *Rev. Geophys.* **50,** doi: 10.1029/2011RG000382.

McGuire, J., and G. Beroza (2012). A rogue earthquake off Sumatra, *Sci. Express* **336,** doi: 10.1126/science.1223983.

Meng, L., J.-P. Ampuero, J. Stock, Z. Duputel, Y. Luo, and V. C. Tsai (2012). Earthquake in a maze: Compressional rupture branching during the 2012 $M_w$ 8.6 Sumatra earthquake, *Science* **337,** 724–726, doi: 10.1126/science.1224030.

Parsons, T. (2005). A hypothesis for delayed dynamic earthquake triggering, *Geophys. Res. Lett.* **32,** L04302, doi: 10.1029/2004GL021811.

Parsons, T., and A. A. Velasco (2011). Absence of remotely triggered large earthquakes beyond the mainshock region, *Nature Geosci.* **4,** 312–316.

Peng, Z., and J. Gomberg (2010). An integrated perspective of the continuum between earthquakes and slow-slip phenomena, *Nature Geosci.* **3,** 599–607.

Pollitz, F., R. S. Stein, V. Sevilgen, and R. Bürgmann (2012). The 11 April 2012 east Indian Ocean earthquake triggered large aftershocks worldwide, *Nature* **490,** 250–253.

Prejean, K., D. P. Hill, E. E. Brodsky, S. E. Hough, M. J. S. Johnston, S. D. Malone, D. H. Oppenheimer, A. M. Pitt, and K. B. Richards-Dinger (2004). Remotely triggered seismicity on the United States west coast following the $M_w$ 7.9 Denali fault earthquake, *Bull. Seismol. Soc. Am.* **94,** S348–S359.

Sevilgen, V., R. Stein, and F. Pollitz (2012). Stress imparted by the great 2004 Sumatra earthquake shut down transforms and activated rifts up to 400 km away in the Andaman Sea, *Proc. Natl. Acad. Sci. Unit. States Am.* **109,** doi: 10.1073/pnas.1208799109.

Shearer, P., and P. Stark (2011). Global risk of big earthquakes has not recently increased, *Proc. Natl. Acad. Sci. Unit. States Am.* **109,** 717–721.

Shelly, D. R., Z. Peng, D. P. Hill, and C. Aiken (2011). Triggered creep as a possible mechanism for delayed dynamic triggering of tremor and earthquakes, *Nature Geosci.* **4,** 384–388.

Storchak, D. A., D. Di Giacomo, I. Bondár, and J. Harris (2012). The ISC-GEM Global Instrumental Reference Earthquake Catalogue (1900–2009), *AGU Fall Meeting*, San Francisco, California.

Tape, C., M. West, V. Silwal, and N. Ruppert (2013). Earthquake nucleation and triggering on an optimally oriented fault, *Earth Planet. Sci. Lett.* **363,** 231–241.

Toda, S., R. S. Stein, G. C. Beroza, and D. Marsan (2012). Aftershocks halted by static stress shadows, *Nature Geosci.* **5,** 410–413, doi: 10.1038/ngeo1465.

van der Elst, N., and E. Brodsky (2010). Connecting near-field and far-field earthquake triggering to dynamic strain, *J. Geophys. Res.* **115,** doi: 10.1029/2009JB006681.

Velasco, A. A., S. Hernandez, T. Parsons, and K. Pankow (2008). Global ubiquity of dynamic earthquake triggering, *Nature Geosci.* **1,** 375–379.

von Huene, R., and D. W. Scholl (2012). Observations at convergent margins concerning sediment subduction, subduction erosion, and the growth of continental crust, *Rev. Geophys.* **29,** 279–316.

Wells, D. L., and K. J. Coppersmith (1994). New empirical relationships among magnitude, rupture length, rupture width, rupture area, and surface displacement, *Bull. Seismol. Soc. Am.* **84,** 974–1002.

Yue, H., T. Lay, and K. D. Koper (2012). En Echelon and orthogonal fault ruptures of the 11 April 2012 great interplate earthquake, *Nature* **490,** 245–249.

# Appendix

## Statistical Model of Global Seismicity

### Conceptual Model

Pollitz *et al.* (2012) proposed the globally propagating seismic waves generated by the Indian Ocean event stressed a sufficient number of close-to-failure patches so that many of them were brought to failure in several $\mathbf{M} \gtrsim 5.5$ events within days of the mainshock. They likened the global seismic response to the shaking of a tree full of apples, some of which were ripe and inevitably shaken down by the seismic waves. Although this idea was motivated by the very low-seismicity rates in the 10 days prior to 11 April 2012, it serves as a useful conceptual model for how many set of potentially failing patches could be brought closer to failure by a transient stress perturbation, that is, propagating seismic waves. We envision that potential nucleation sites are in randomly distributed states between being relaxed (presumably after their last significant rupture) and being critically stressed. And these sites age at a constant rate (assuming constant background tectonic stressing). A consequence of

these simple assumptions is that if the reservoir of close-to-failure sites is perturbed by bringing a number of those sites to failure within a short time (i.e., shortly after a dynamic stress perturbation), then fewer sites will be available for failure in the subsequent period.

To quantify this model, we suppose that there are $N$ patches distributed globally that may fail in an $\mathbf{M} \geq 6.5$ event. On these patches we assume an average strain accumulation rate $\dot{\epsilon}$, strain release $\Delta\epsilon$, and average combined rate of rupture $\lambda$. Let $\{\epsilon_i, i = 1, \ldots, N\}$ be the patch strains. From their rate of combined rupture, these strains are randomly distributed such that within a time interval $\Delta T$, the probability of a rupture on the collection of patches is

$$\prod_{i=1}^{N} P[\epsilon_i - \epsilon_{\text{crit}} < \dot{\epsilon}\Delta T] = e^{-\lambda\Delta T}, \tag{A1}$$

in which $\epsilon_{\text{crit}}$ ($> \epsilon_i$ for all $i$) is a critical strain threshold such that rupture on a given patch will occur when strain builds up to that value. Equation (A1) states that in a Poissonian model of earthquake occurrence on a collection of faults, the probability of having an interval $\Delta T$ without an event is $e^{-\lambda\Delta T}$, in which $1/\lambda$ is the mean interevent time. Assuming the $\{\epsilon_i\}$ is identically distributed, for one patch we have

$$P[\epsilon_i - \epsilon_{\text{crit}} < -\dot{\epsilon}\Delta T] = e^{-\lambda\Delta T/N}. \tag{A2}$$

## Short-Term Triggering

We hypothesize that transient strains from the April 2012 event led to short-term rupture of a fraction $f_1$ of available patches that were within $\epsilon_{\text{d}}$ of failure; these would correspond to the four $\mathbf{M} \geq 6.5$ events that actually occurred during the first 10 postseismic days (Figs. 1d, 3b). We choose $\epsilon_{\text{d}} = 0.1\mu$ strain based on the order of magnitude of the amplitude of transient strains transmitted globally (Pollitz *et al.*, 2012). Define $L$ to be the number of $\mathbf{M} \geq 6.5$ patches expected to be within $\epsilon_{\text{d}}$ of failure upon the occurrence of the April 2012 event, so that the number of patches that ruptured in the short term is $Lf_1$. If strain states are randomly distributed between $\epsilon_{\text{crit}} - \Delta\epsilon$ and $\epsilon_{\text{crit}}$, then

$$L = N\frac{\epsilon_{\text{d}}}{\Delta\epsilon}. \tag{A3}$$

Equation (A3) is consistent with the empirical result that the number of far-field triggered events tends to scale linearly with the amplitude of the peak dynamic strain (van der Elst and Brodsky, 2010). Because patches undergo a strain drop $\Delta\epsilon$ when they fail, the left side of equation (A2) is $\exp(-\dot{\epsilon}\Delta T/\Delta\epsilon)$. Equating this with the right side of equation (A2) yields

$$N = \lambda\frac{\Delta\epsilon}{\dot{\epsilon}}, \tag{A4}$$

which, combined with equation (A3) yields

$$L = \lambda\frac{\epsilon_{\text{d}}}{\dot{\epsilon}}. \tag{A5}$$

## Longer-Term Quiescence

The global system yields $Lf_1$ short-term triggered events. These events are by themselves insufficient to account for the budget of expected $\mathbf{M} \geq 6.5$ events within 105 days following the Indian Ocean mainshock. As discussed in the Postmainshock Quiescence section, Figure 6 implies an apparent 5.4-earthquake gap between the expected number of events during the 10–105 days period (94 events) and the four that actually occurred. If this arithmetic were correct, then the quiescence is roughly twice as long as would be expected for the number of short-term (triggered) $\mathbf{M} \geq 6.5$ events. However, if these four events were considered as a separate phenomenon, that is, dynamically triggered events, not part of the budget of expected $\mathbf{M} \geq 6.5$ events, then there would be an even larger gap in the number of $\mathbf{M} \geq 6.5$ events expected to occur during the first 105 postmainshock days—8.4 events as indicated in Figure 6.

As we are dealing with the statistics of small numbers, any observed gap may be a random, albeit rare, statistical fluctuation with no physical underpinnings. The alternative would be to propose that after the April 2012 mainshock, a fraction $f_2$ of the remaining $L \times (1 - f_1)$ close-to-failure patches was made ineligible for rupture, notwithstanding their strain state, by some process associated with dynamic stressing from the mainshock. We may interpret the $T_{\text{quiet}} =$ 95 day interval without $\mathbf{M} \geq 6.5$ events as the amount of time that the reset system needed to have a probability $1 - \exp(-1)$ of producing an event. Specifically,

$$\prod_{i=1}^{L(1-f_1)(1-f_2)} P[\epsilon_i - \epsilon_{\text{crit}} < -\dot{\epsilon}T_{\text{quiet}}] = e^{-1}. \tag{A6}$$

Note that equation (A6) accounts for the occurrence of the $Lf_1$ events during the initial short-term activity. Assuming that these eligible $L(1 - f_1)(1 - f_2)$ close-to-failure patches are identically distributed, for one patch we have

$$P[\epsilon_i - \epsilon_{\text{crit}} < -\dot{\epsilon}T_{\text{quiet}}] = e^{-1/[L(1-f_1)(1-f_2)]}. \tag{A7}$$

If these $\epsilon_i$ are uniformly distributed over the interval $(\epsilon_{\text{crit}} - \epsilon_{\text{d}},\ \epsilon_{\text{crit}})$, then the left side of equation (A7) is $\exp[-\dot{\epsilon}T_{\text{quiet}}/\epsilon_{\text{d}}]$. Equating this with the right side of equation (A7) yields

$$L(1 - f_1)(1 - f_2) = \frac{1}{T_{\text{quiet}}}\frac{\epsilon_{\text{d}}}{\dot{\epsilon}}. \tag{A8}$$

Substituting equation (A5) for $L$ into equation (A8) yields

$$f_2 = 1 - \frac{1}{1 - f_1}\frac{1}{\lambda T_{\text{quiet}}}. \tag{A9}$$

Combining equations (A5) and (A9) with the constraint $Lf_1 = 4$ (the number of short-term triggered events, i.e. Figs. 1d and 3b), we may solve for $L$, $f_1$, and $f_2$. Using parameter values $\dot{\epsilon} = 0.05\mu$ strain/year and $\epsilon_d = 0.1\mu$ strain, this yields $L = 66$, $f_1 = 0.061$, and $f_2 = 0.88$. The estimate of $L$ is sensible, as it represents the number of patches that are within 0.1 $\mu$ strain of failure with a loading rate of 0.05 $\mu$ strain/year, that is, the number of nucleation sites that ripen in a two year time interval. We expect 66 $\mathbf{M} \geq$ 6.5 events to occur within an average two-year timespan given the occurrence rate of $\lambda = 0.089$/day.

## Discussion

The total number of $\mathbf{M} \geq 6.5$ source patches $N$ is given by equation (A4) for a suitable choice of $\Delta\epsilon$. A typical stress drop of 3 MPa corresponds to $\Delta\epsilon = 50\mu$ strain, leading to $N = 32{,}800$ total source patches. The fault area corresponding to $\mathbf{M} = 6.5$ is 164 km$^2$ (Wells and Coppersmith, 1994), so the minimum area of our idealized system is $5.4 \times 10^6$ km$^2$ (minimum because fault area is larger for $\mathbf{M} > 6.5$). This is comparable with the total area along the seismogenic portion of the worlds's subduction zones and transform faults. A total length of the global subduction zones of 43,500 km (von Huene and Scholl, 2012) times 150 km downdip distance yields $6.5 \times 10^6$ km$^2$. A total length of transform faults of 44,433 km (Bird *et al.*, 2002) times a mean coupled lithosphere thickness of 3 km (Bird *et al.*, 2002) yields $0.1 \times 10^6$ km$^2$, for a total of $6.6 \times 10^6$ km$^2$ The fault area calculated from our simple statistical model is approximately the area of active faults that was subject to high-transient strain.

Equation (A9) states that the fraction $f_2$ of inhibited patches is larger when the product $\lambda T_{quiet}$ is larger. The latter is simply the 8.4 earthquake gap illustrated in Figure 6. The equation also states that $1 - f_2$ is inversely proportional to $1 - f_1$, so if a larger fraction of available ripe nucleation patches had ruptured in the short term, $f_1$ would be larger and $f_2$ would be correspondingly smaller. Because inferred $f_1$ is small, the four events that occurred in the short term are only a small fraction of the nucleation sites that were probably close to failure. In other words, the occurrence of these four events removed an insignificant number of sites from the pool of close-to-failure sites.

The fraction of inhibited ruptures would be smaller if the number of close-to-failure sites $L$ was smaller than prescribed by equation (A5), as would be the case if $\mathbf{M} \geq 6.5$ earthquake productivity were unusually high for a long period before the 11 April 2012 event. However, the premainshock productivity appears no different from the 30 year background level (Fig. 6). The fraction of inhibited ruptures would also be smaller if it were supposed that the short-term triggered events represented those patches closest to rupture at the time of the 11 April 2012 mainshock, that is, those next in line to rupture had the 11 April 2012 event not occurred. In that case, our analysis would still require a fraction $f_2 = 1 - 1/(5.4\,\text{events}) = 81\%$ to have been inhibited from rupture, consistent with the 5.4 event gap depicted in Figure 6. We conclude that regardless of its effective size, the 5 to 9 earthquake gap accumulated over the 105 day period following the 11 April 2012 mainshock is either statistically uncertain, or needs to be accounted for by inhibiting rupture of nucleation sites that would have been expected to ripen during this time.

U.S. Geological Survey
345 Middlefield Rd., MS 977
Menlo Park, California 94025
(F.F.P., R.S.S., V.S.)

Department of Earth and Planetary Science
University of California
389 McCone Hall
Berkeley, California 94720-4767
(R.B.)

Manuscript received 3 April 2013;
Published Online 11 March 2014